Improving ALD-Al2O3 Surface Passivation of Si using Native SiO_x

Michael N. Getz (michael.getz@fys.uio.no)
University of Oslo, Department of Physics
Marco Povoli
Department of Microsystems and Nanotechnology (MiNaLab), SINTEF Digital, Oslo
Eduard Monakhov
University of Oslo, Department of Physics

Research Article

Keywords: surface passivation,native silicon oxide, optimal deposition temperature Al2O3, Al2O3 growth rate, TMA + O3 + H2O ALD, Effect of HF-dip, long-term stability Al2O3

Posted Date: October 4th, 2021

DOI: https://doi.org/10.21203/rs.3.rs-943524/v1

Abstract

Al_2O_3 has rapidly become the surface passivation material of choice for the n-type Si solar cells with p + emitter due to its high negative fixed charge, good long-term and thermal stability, and no parasitic absorption. In this study, the surface saturation current density, fixed charge, and interface state density is compared for Al_2O_3 grown on Si substrates where the native SiO_x was not removed, with substrates where the SiO_x was removed by hydrofluoric acid. The depositions are performed by atomic layer deposition at temperatures in the 150–300 ˚C range, using trimethylaluminium, H_2O, and O_3 as precursors. The samples where the native oxide was not removed achieve a higher level of surface passivation for every tested deposition temperature, with the sample deposited at 200 ˚C exhibiting a surface saturation current density of only 1.9 fA/cm^2, a fixed charge of 4.2×10^{12} cm^{-2}, and a density of interface states of 9.8×10^{9} cm^{-2} ev^{-1}. Capacitance and conductance voltage characteristics reveal a strong correlation between the surface saturation current density and the density of interface states and fixed charges. It is also determined that the long-term stability of the surface passivation depends on the deposition temperature, with higher deposition temperatures resulting in improved long-term stability.

1. Introduction

Al_2O_3 deposited by atomic layer deposition (ALD) or plasma enhanced chemical vapour deposition (PECVD) has become the industry material of choice for surface passivation of commercial Si solar cells, [1] due to its high negative fixed charge being suitable for passivating the p + emitter of n-type Si,[2–8] while also exhibiting excellent thermal, long-term, and UV-stability.[9–10] The PECVD-Al_2O_3/SiN_x stack is currently dominating the market, however, ALD-Al_2O_3 with PECVD SiN_x capping layer is gaining market shares and is projected to have an almost 50% market share by 2030.[1]

Al_2O_3 has an oxygen rich AlO_x interface layer with negatively charged oxygen interstitials and Al vacancies, as well as oxygen dangling bonds, shown by density functional calculations to form charge-state transition levels well below the valence band edge of silicon that can accept electrons from the singly-occupied dangling Si bonds.[11] Hiller et al. have also demonstrated that electrically active surface states of silicon can be deactivated by Al-induced acceptor states in SiO_2 in a similar manner.[12–13] The fixed charges created in this way will be compensated by an equal positive charge in the silicon, and do not directly repel charges away from the interface, however, the number of trapped electrons in the SiO_x-Al_2O_3 interface layer is large, with $Q_{fix} > 10^{12}$ cm^{-2},[3, 14–16] implying that the number of electrons near the surface region of silicon is significantly reduced, thereby sharply reducing the probability of electron-hole recombination in the same way as a p^+ layer in p-type Si does.[17] Annealing at > 400 ˚C in N_2, forming gas (FG), or O_2, reduces D_{it} from > 10^{12} ev^1 cm^2 to < 10^{11} ev^1 cm^2,[3, 14–16] commonly attributed to either hydrogen diffusion towards the Si-SiO_x interface passivating the Si dangling bonds near the surface and in the bulk, or by increased SiO_x formation between Si and Al_2O_3.[2–4, 18–19] However, von Gastrov et al.[20] have demonstrated that Al_2O_3 prepared using O_3 contains less hydrogen and more carbon than samples

made using H_2O, yet exhibit significantly improved surface passivation post annealing, which thus has to be attributed to the increased negative fixed charge observed in these samples rather than to chemical passivation by hydrogen.

The oxygen rich interface layer of Al_2O_3 has been attributed to tetrahedrally coordinated Al in AlO_4^- that is formed due to the tetrahedral coordination of Si in the 0.5-2 nm SiO_x layer that is unintentionally formed primarily during the $H_2O/O_3/O_2$ plasma pulses of the initial ALD cycles.[2, 21–22] The SiO_x layer is thus considered critical to the formation of fixed charges in Al_2O_3, and improved understanding of the role of this layer could help reduce costs and increase efficiencies even further.

Al_2O_3 is commonly deposited by thermal ALD using trimethylaluminium (TMA) and H_2O or O_3,[3, 5, 23] however, a combination of H_2O and O_3 has previously been shown to yield very low surface recombination velocities post annealing,[20] which can be attributed to the high Q_{fix} associated with using O_3, combined with low carbon concentration associated with using H_2O, resulting in both high Q_{fix} and low D_{it}. Surface recombination velocities can generally be reduced by increasing film thickness, however, > 10 nm film thickness has been shown to provide only small improvements in surface passivation.[24]

Using the $H_2O + O_3$ combination as oxygen precursors, we previously demonstrated superior surface passivation for Al_2O_3 grown on as-received wafers with the native oxide present, compared to wafers subjected to a 3 min HF-dip prior to the ALD deposition at 150 ˚C.[25] In this study, the aim has been to investigate if using a native oxide is beneficial still at higher deposition temperatures, and to determine the optimal process parameters with respect to reducing the surface saturation current density, J_{0s}, considered to be the most useful metric to quantify surface passivation of dielectrics with high Q_{fix}.[26] We also investigate how the deposition temperature and pre-treatment affects the long-term stability.

2. Experimental

The substrates that were used for impedance measurements were cut from single-side polished (SSP) p-type 525 ± 20 µm < 100 > oriented silicon wafers with a doping level of 1.8–2.0 × 10^{16} cm^{-3} from Siegert Wafer. Half of the substrates received no further pretreatment, referred to as “no-HF” from here on, while the other half of the substrates were submerged in 2% HF solution for 3 min, followed by a ca. 1 min bubble rinse in DI water, referred to as “HF-dipped” from here on. The unpolished side (back side) of all the substrates were contacted with ca. 180 nm Al by thermal evaporation.

For lifetime measurements, 12 cm^2 substrates were cut from double-side polished (DSP) p-type 500 µm < 100 > oriented silicon wafers with a reported resistivity of > 5 kΩ □ cm from Topsil. Half of the substrates were subjected to the HF-dip pretreatment, while the other half received no pretreatment.

A Beneq TFS-200 ALD reactor was used for the Al_2O_3 deposition by using trimethyl-aluminium (TMA) (99.999%) from Strem chemicals, H_2O and O_3, with a pulse duration of 0.4/2/0.4/2/1/2.5 s for 145 cycles

of TMA/N_2/H_2O/N_2/O_3/N_2, respectively. The depositions were carried out with background pressure of 2 mbar and deposition temperatures of 150, 200, 250, and 300 ˚C. The depositions were preceded by an *in-situ* 5 min O_3 pre-treatment (30 cycles of 1 s O_3/ 9 s N_2) at the deposition temperature to remove potential organic contaminants and flush the O_3 line and improve the surface reactivity towards TMA. For each deposition temperature, one HF-dipped and one no-HF substrate was loaded into the reactor. Each deposition was performed twice, once for the SSP substrates that were only coated on one side, and once more for the DSP substrates that were coated simultaneously on both sides.

Native SiO_x and deposited Al_2O_3 film thicknesses were determined with a J. A. Woollam ellipsometer in the 380–890 nm range. The spectroscopic ellipsometry (SE) experimental data of the samples prior to deposition was fitted using the native silicon oxide model provided by the CompleteEASE software, which uses optical constants determined by Herzinger, et al.[27]. The Cauchy-model was used to parameterize the SE data of the films after deposition. Three measurements were performed at different locations on the surfaces of samples. The uncertainty provided in the reported thicknesses reflect the different thicknesses measured across the surface and includes the uncertainties in the fitted values.

Annealing was performed in a tube furnace at 435 ˚C for 10 min in FG (10% H_2). The temperature at the sample position was monitored with an external thermocouple.

Ca. 180 nm thick circular Al gate electrodes were deposited using shadow masks with hole diameters of ca. 1 mm by thermal evaporation. A contact area of 0.709 mm^2 was deduced from optical microscopy and this value is used for the calculations performed in this study.

The capacitance-voltage (CV) characteristics and conductance-voltage (GV) characteristics were recorded at various probe frequencies in the range of 500 Hz to 250 kHz, with an oscillation voltage of 30 mV using Precision Impedance LCR Analyzer (4284A, Agilent Technologies) in parallel conductance mode. The samples were briefly illuminated prior to the voltage sweep, which were performed in darkness. The gate voltage was swept at room temperature from depletion (-5 V) to accumulation (3 V) and back again at a rate of 0.02 V/s. Note that the presented figures shows the G/ω vs. V characteristics, but are referred to as GV characteristics for brevity.

The effective minority carrier lifetimes of the as-deposited and post annealed samples were recorded using a Sinton Instruments WCT-120 with the generalized quasi-static photoconductance (QSSPC) mode for the as-deposited samples, and the transient photoconductance decay (PCD) mode for the annealed samples. The sample stage was kept at 25˚C. The measurements of the annealed samples were performed after the sample temperature cooled down to ca. 25 ˚C, ca. 10 min after they were extracted from the furnace.

3. Results

The thicknesses obtained by SE for the samples before and after deposition are provided in Table S1 and S2. Due to the similarities in refractive index of SiO_x and Al_2O_3 in the amorphous state, SE measurements will yield the total dielectric thickness,[28] the growth per cycle (GPC) presented in Fig. 1 has therefor been calculated for films deposited on SSP substrates after subtracting the thickness measured by SE prior to deposition. There is no literature

describing the growth rate of the TMA + H_2O + O_3 system, however, the growth rates are in close agreement with those observed for TMA + O_2 plasma.[29] The apparent increased growth rate of HF-dipped samples relative to the no-HF samples is attributed to formation of SiO_x during the initial ALD-cycles, as previously demonstrated by transmission electron microscopy (TEM).[2, 21–22] There is little or no significant difference in total film thickness between HF-dipped and no-HF samples when deposited at the same deposition temperature. This indicates that the thickness of the SiO_x layer that forms on HF-dipped samples during the deposition is similar to the native SiO_x thickness of ca. 1.6 nm (Table S1), provided that little or no further SiO_x is formed on no-HF samples.

3.1 Lifetime measurements

The effective lifetime in the as-deposited no-HF and HF-dippped samples is presented in Fig. 2. The no-HF samples consistently exhibit lifetimes at least one order of magnitude longer than the HF-dipped samples for all deposition temperatures, T_{dep}, over the recorded injection level range. The sample deposited at 300 ˚C exhibits the longest lifetime in the as-deposited state, which is attributed to the deposition temperature having an effect similar to that of annealing.

Post FG annealing, the lifetime improves significantly for all samples, as shown in Fig. 3a and 3b for no-HF and HF-dipped samples, respectively. J_{0s} was deduced from the linear fit of the linear region of inverse lifetime data at high injection, shown for no-HF and HF-dipped samples in Fig. 3c and 3d, respectively, using the Kane-Swanson slope method:[30]

$$\frac{1}{\tau_{eff}} = \frac{1}{\tau_{Auger}} + \frac{1}{\tau_{SRH}} + 2\frac{J_{0s}}{q n_i W^a}\left(\frac{(N_a^{(1)} + \Delta n)}{}\right)$$

where τ_{eff} is the measured effective excess carrier lifetime, τ_{Auger} is the intrinsic Auger lifetime,[31] τ_{SRH} is the defect-related bulk lifetime, N_a is the base doping level, Δn is the excess carrier density, q is the elementary charge, n_i is the intrinsic carrier concentration (8.305×10^9 cm^{-3} at 298.15 K),

and W is the wafer thickness. The no-HF samples exhibit consistently lower J_{0s} at each deposition temperature, suggesting that the findings reported previously at 150 ˚C are qualitatively valid for all deposition temperatures.[25] The lowest J_{0s} is observed for deposition temperatures of 200 ˚ C for both no-HF and HF-dipped, with the no-HF sample exhibiting J_{0s} = 1.9 fA/cm^2.

Figure 4 shows how J_{0s} changes for each sample after8 months of storage while wrapped in Al-foil inside a zip-lock bag in a cleanroom. The corresponding lifetimedata used to determine$J_{0s}$are available in Figure S1.The surface passivation provided by ALD-Al_2O_3 has previously been reported to be stable over time, and in some cases an improvement over time is observed.[3, 10] The results in this study indicate that the long-term stability depends on the deposition temperature. All samples in this study exhibit some reduction in lifetime at the 1×10^{15} cm^{-3}injection level,

particularly severe for samples deposited at 150 ˚C and 200 ˚C, where J_{0s} increased by ~ 50% for all samples. However, due to the low initial J_{0s} of the no-HF sample deposited at 200 ˚C, this only amounts to a 1 fA/cm^2 increase and can thus be said to be reasonably stable in absolute terms. For samples deposited at 250 ˚C, J_{0s} increased by less than 10%, while for both samples deposited at 300 ˚C, J_{0s} was reduced by ca. 40%. The improvement in J_{0s} for samples deposited at 300 ˚C is indicative of some form of structural change taking place after annealing. Notably, the long-term stability does not appear to be affected by the pretreatment, indicating that the observed changes are related to the Al_2O_3 and not to the SiO_x interface layer. No further changes in the lifetime or J_{0s} were observed in the two weeks following the 8 months of storage, indicating that the films have become stable. Annealing an HF-dipped sample deposited at 150 ˚C again after aging had no effect on the lifetime.

Despite the significantly improved surface passivation of the samples deposited at 300 ˚C, they still perform worse than samples deposited at 200 ˚C, which appears to be the optimal deposition temperature when depositing on native SiO_x and taking long-term stability into account. 200 ˚C was also determined to be the optimal deposition temperature for HF-dipped samples, in agreement with previous studies.[6, 32–33]

3.2 Capacitance-Voltage and Conductance-Voltage characteristics

Q_{fix} and D_{it} were estimated from impedance measurements using parallel conductance mode. Series resistance correction was performed according to the method described in the supplementary material. Figure 5a and b respectively show the corrected CV and GV characteristics of the no-HF sample deposited at 200 ˚C in the as-deposited state, while the CV and GV characteristics of the annealed sample is presented in Fig. 5c and d, respectively.

Q_{fix} can be approximated to be equal to the effective charge, Q_{eff}, obtained from CV characteristics, provided that the contribution from fixed charges is much larger than contributions from other charges. This is a reasonable assumption if the number of mobile charges is small and if the measurement is performed at high frequency (hf), as the filling and emptying of interfacial traps is too slow to follow at high frequencies and will eventually no longer contribute to the CV

signal. The as-deposited samples contain a large number of interfacial traps and the highest frequency used in this study, 250 kHz, was not sufficient to completely avoid contributions from interfacial traps,

however, considering the clear exponential dependence of the flatband voltage, V_{FB}, on the frequency in Fig. 5a, it is possible to estimate Q_{eff} for a given frequency by fitting the resulting data points to a double exponential.[25] Using this approach and letting f approach infinity for the data in Fig. 5a, $Q_{eff}(hf) \approx 4.6 \times 10^{12}$ cm^{-2} is obtained (fit is available in Figure S2).

The contribution from mobile charges is typically estimated from the hysteresis that arises by first sweeping the voltage from inversion to accumulation and then back again to inversion at 250 kHz (shown for the no-HF sample deposited at 200 ˚C, post annealing, in Figure S3). The hysteresis at the flatband capacitance, C_{FB}, was 37 mV, indicating that the contribution from mobile charges can be assumed to be negligible to the total shift in V_{FB} of ca. 2 V relative to built-in potential, φ_{ms}, so that the approximation $Q_{eff}(hf) \approx Q_{fix}$ appears to be reasonable. For the as-deposited samples, the hysteresis at C_{FB} is in the range of 100–200 mV, so the contribution is more significant, and the reported Q_{fix} value must thus be considered to be a significant overestimation for the as-deposited samples. Nevertheless, the obtained values are in agreement with previously reported values of Q_{fix} for Al_2O_3 (10^{11-13} cm^2).[3, 15, 34]

D_{it} was determined using the conductance method devised by Hill and Coleman:[35]

$$D_{\mathrm{it}} = \frac{2.5}{qA\left(\frac{\max\left(\frac{G}{\omega}\right)}{C_{\mathrm{ox}}}\right)^2 + (1-\theta^2)} \tag{9}$$

where max(G/ω) is the peak value of the largest peak in Fig. 5b and d, and C is the corresponding capacitance at that voltage. D_{it} for the as-deposited films deposited at 200 ˚C was determined to be 2.4 × 10^{12} and 2.1 × 10^{12} ev^{-1} cm^{-2} for the HF-dipped and no-HF samples, respectively. The values are in agreement with previously reported values for as-deposited Al_2O_3.[36–37] Note that with max(G/ω) occurring at the lowest frequency used, i.e. 500 Hz, it is likely that the actual maximum is at a lower frequency, and the reported D_{it} values may thus be slightly underestimated.

Post annealing, the D_{it} was determined to be 2.8 × 10^{10} and 9.8 × 10^9 ev^{-1} cm^{-2} for the HF-dipped and no-HF samples deposited at 200 ˚C, respectively, with the no-HF sample exhibiting the lowest D_{it} among the samples in this study. The two peaks in the GV characteristics of the annealed no-HF sample (5d) is a result of two similarly populated defect levels that respond differently to the frequency. The other samples only exhibit one significant peak with max(G/ω) at 500 Hz, shown for the samples deposited at 250 ˚C in Figure S4. The 500 Hz peak was consequently used for D_{it} extraction for all samples (Figure S5).

Figure 6a shows the obtained Q_{fix} of all samples, while the corresponding D_{it} of the samples are presented in Fig. 6b. The exact values are available in Table S3 and S4. The no-HF samples consistently exhibit lower D_{it} values and equal or more Q_{fix}, in agreement with the reduced J_{0s} of no-HF samples

relative to HF-dipped samples observed from the PCD measurements in Fig. 3. Figure 6 also shows that D_{it} increases for deposition temperatures > 200 ˚C. We did not observe any significant changes in the CV or GV characteristics over time for any of the samples. The apparent decrease in Q_{fix} post annealing can partially be attributed to the overestimation of the Q_{fix} in the as-deposited samples due to mobile charges.

4. Discussion

Both the results from PCD and impedance measurements demonstrate that the no-HF samples exhibit superior surface passivation to the HF-dipped samples when comparing samples deposited at the same deposition temperature. We previously demonstrated this for samples deposited at 150 ˚C,[25] and the present study indicates that this is generally true for deposition temperatures in the 150–300 ˚C range for the TMA + H_2O + O_3 process. Importantly, this includes depositions at 200 ˚C, previously determined to be the optimal deposition temperature,[6, 32–33] where the no-HF sample exhibits more than three times lower J_{0s} post annealing, which CV and GV characteristics indicate is due to an almost three times lower D_{it} and slightly increased Q_{fix}.

A possible reason for the HF-dipped samples performing worse than the ones with a native SiO_x layer is likely related to the differences in the reaction of TMA with Si-H and Si-OH. We previously proposed Al and C may be incorporated into the SiO_x layer that is formed during the initial ALD cycles on H-terminated Si.[25] We will elaborate a bit further on this here.

A key difference in depositing on native SiO_x and H-terminated Si is the reaction mechanisms during the initial ALD cycles. Previous studies have shown that while steady-state growth of 4 Al/nm^2 occurs already after the first ALD cycle on OH-terminated SiO_x, only ca. 0.1 Al/nm^2 is deposited during the first ALD cycle on H-terminated Si at 300 ˚C, which increases to the steady-state growth rate after ca. 15–20 cycles.[21, 38–39] During the first TMA cycle, *in-situ* transmission infra-red spectroscopy has shown only small reductions in Si-H bonds, while significant Si-CH_3 and small amounts of Al-CH_3 bond formation is observed.[40] Only the Al-CH_3 species are reactive towards H_2O, so in the subsequent H_2O pulse, Si-Al-OH species are formed only at these locations. The Al-OH species are highly reactive towards TMA, which can result in island growth formation of Al_2O_3, as previously indicated by TEM.[39] Most of the Si-CH_3 species can eventually become hydrolysed by neighbouring Al-OH species once the coverage of Al-OH is large enough,[40] and the H-terminated Si will eventually also become oxidized during the H_2O and O_3 pulses. The oxidation of H-terminated Si by H_2O has been studied in detail previously, and it is believed that Si-OH and H_2 is formed initially, and that the OH- group then inserts into a Si-Si back bond, creating Si-O-Si and regenerates a Si-H bond at the surface, which then reacts with more H_2O.[41–42] The low growth rates are thus likely to result in an AlO_x layer with a different structure and density than an AlO_x layer growing at steady state growth conditions after the first cycle. The 0.5-2 nm SiO_x layer that is formed during the deposition, as demonstrated by TEM of as-deposited samples,[2, 21–22] is formed while

Si-CH_3 and Si-Al-CH_3 is covering the surface, likely causing significant amounts of both Al and C to be incorporated into the SiO_x layer. Annealing should enable the rearrangement of the interface atoms in a way that reduces the high energy associated with dangling bonds and uncompensated charges in the disordered SiO_x-AlO_x layer, which could explain why the difference in lifetime between HF-dipped and no-HF samples is more than an order of magnitude different as-deposited, while it is much less after annealing. However, annealing may also cause Al to diffuse into the SiO_x layer, particularly if the SiO_x layer is highly disordered.[43] Secondary ion mass spectrometry of an annealed ALD Al_2O_3 film deposited on H-terminated Si has also previously shown that at the depth where1/3 of the detected atoms are Si, which would be expected from tetrahedrally coordinated Si in SiO_2, 1/5 of the detected atoms are Al, thus revealing large amounts of Al in the SiO_x layer.[44] As the fixed negative charge of Al_2O_3 is primarily attributed to an oxygen rich layer with O interstitials and Al vacancies with tetrahedrally coordinated Al that is prevalent partly due to the tetrahedrally coordinated Si in SiO_x,[11–12] it is not surprising if large amounts of Al in the SiO_x layer may have a detrimental effect, and thus can explain the slightly reduced negative Q_{fix} observed in HF-dipped samples relative to no-HF samples. Al impurities are also associated with increased D_{it}.[45]

As the native oxide of the no-HF samples has not been formed in the presence of Si-Al-CH_3, it likely has a lower aluminum concentration, and possibly lower carbon concentration, depending on the conditions in which the native SiO_x was formed, which thus could explain the significantly reduced J_{0s}. More research is necessary in order to completely understand how the SiO_x layer formation influences Q_{fix} and D_{it}, however, the results indicate that an excellent level of surface passivation can be achieved by depositing 20 nm Al_2O_3 using a mixture of H_2O and O_3 at a deposition temperature of 200 ˚C on ca. 1.6 nm of native SiO_x, with a J_{0s} of only 1.9 fA/cm^2 ca. 10 min after annealing for 10 min in FG at 435 ˚C. J_{0s} values for single-layer Al_2O_3 has previously been reported to be 8 fA/cm^2 on 226 Ω/□ wafers by Richter et al.[46], 10 fA/cm^2 on > 100 Ω/□ by Hoex et al.[14], and 23 fA/cm^2 on 140 Ω/□, by Benick et al.[47] The wafers used in this study have sheet resistance of > 1000 Ω/□, so a lower J_{0s} is to be expected and a direct comparison cannot be made, however, increasing sheet resistances beyond 200 Ω/□ should only have a small effect on J_{0s},[8] indicating that the process is likely to still be an improvement over previously reported results, which is also supported by the exceptionally low D_{it} and high Q_{fix} of the similarly processed sample.

The temperature dependence of the long term stability of the surface passivation was unaffected by the pretreatment and is thus more likely to depend on the Al_2O_3 layer itself. The decrease in GPC observed with increasing deposition temperature is associated with an increased film density,[48] which thus may be related to the observed differences in long term stability.

5. Conclusion

We have demonstrated that the TMA + H_2O + O_3 ALD process results in excellent surface passivation of p-type Si when followed by FGA at 435 ˚C for 10 min. The highest level of surface passivation was achieved for a sample where the native oxide layer was not removed prior to Al_2O_3 deposition carried out at 200 ˚C, resulting in J_{0s} of 1.9 fA/cm^2. CV and GV revealed that the sample processed in the same way exhibited the lowest D_{it} of 9.8 × 10^9 ev^{-1} cm^{-2} and the highest Q_{fix} of -4.2 × 10^{12} cm^{-2} among the annealed samples investigated in this study. For every deposition temperature, samples subjected to a 3 min HF-dip consistently exhibited higher J_{0s} and D_{it} than samples where the native SiO_x layer was not removed prior to deposition. Samples deposited at 150 and 200 ˚C exhibited a ca. 50% increase in J_{0s} after 8 months of cleanroom storage after annealing, while for samples deposited at 250 ˚C, a less than 10% reduction was observed. For samples deposited at 300 ˚C, J_{0s} was reduced by ca. 40%. The long-term stability was independent of the HF pretreatment. Due to the low initial J_{0s} of samples deposited at 200 ˚C, these samples still exhibited significantly lower J_{0s} compared to similarly processed samples deposited at other temperatures.

Declarations

Supplementary material

See supplementary material for additional sample information, measurement data, and additional data fitting that supports the findings in the article.

Data availability

The data that support the findings of this study are available from the corresponding author upon reasonable request.

Acknowledgements and funding

This research was funded, in whole or in part, by The Research Council of Norway (Grant No. 289437). A CC BY or equivalent license is applied to any Author Accepted Manuscript (AAM) version arising from this submission, in accordance with the grant's open access conditions. The Research Council of Norway is acknowledged for support to the Norwegian Micro- and Nano-Fabrication Facility, NorFab (Project No. 295864).

Conflict of Interest

The authors declare no conflict of interest.

References

[1] M. Fischer, M. Woodhouse, S. Herritsch, J. Trube, International Technology Roadmap for Photovoltaic (ITRPV) 2020 Results, **2020** (VDMA Photovoltaic Equipment).

[2] B. Hoex, S. B. S. Heil, E. Langereis, M. C. M. v. d. Sanden, W. M. M. Kessels, *Appl. Phys. Lett.* **2006**, *89*, 042112.

[3] G. Dingemans, W. M. M. Kessels, *J. Vac. Sci. Technol. A* **2012**, *30*, 040802.

[4] J. Schmidt, B. Veith, R. Brendel, *Phys. Status Solidi Rapid Res. Lett.* **2009**, *3*, 287-289.

[5] D. K. Simon, P. M. Jordan, I. Dirnstorfer, F. Benner, C. Richter, T. Mikolajick, *Sol. Energy Mater. Sol. Cells* **2014**, *131*, 72-76.

[6] N. Batra, J. Gope, Vandana, J. Panigrahi, R. Singh, P. Singh, *AIP Adv.* **2015**, *5*, 067113.

[7] R. S. Bonilla, B. Hoex, P. Hamer, P. R. Wilshaw, *Phys. Status Solidi A* **2017**, *214*, 1700293.

[8] J. Schmidt, R. Peibst, R. Brendel, *Sol. Energy Mater. Sol. Cells* **2018**, *187*, 39-54.

[9] J. Schmidt, A. Merkle, R. Bock, P. Altermatt, A. Cuevas, N. Harder, B. Hoex, M. C. M. Sanden, W. M. M. Kessels, R. Brendel, Progress in the surface passivation of silicon solar cells, Proceedings 23rd European Photovoltaic Solar Energy Conference, Valencia, Spain, **2008**, pp. 2DP.2.4-974-981.

[10] G. Dingemans, P. Engelhart, R. Seguin, F. Einsele, B. Hoex, V. d. Sanden, W. Kessels, *J. Appl. Phys.* **2009**, *106*, 114907.

[11] B. Shin, J. R. Weber, R. D. Long, P. K. Hurley, C. G. V. d. Walle, P. C. McIntyre, *Appl. Phys. Lett.* **2010**, *96*, 152908.

[12] D. Hiller, P. M. Jordan, K. Ding, M. Pomaska, T. Mikolajick, D. König, *J. Appl. Phys.* **2019**, *125*, 015301.

[13] D. König, D. Hiller, S. Gutsch, M. Zacharias, S. Smith, *Sci. Rep.* **2017**, *7*, 46703.

[14] B. Hoex, J. Schmidt, R. Bock, P. P. Altermatt, M. C. M. v. d. Sanden, W. M. M. Kessels, *Appl. Phys. Lett.* **2007**, *91*, 112107.

[15] D. K. Simon, P. M. Jordan, T. Mikolajick, I. Dirnstorfer, *ACS Appl. Mater. Interfaces* **2015**, *7*, 28215-28222.

[16] T. Niewelt, A. Richter, T. C. Kho, N. E. Grant, R. S. Bonilla, B. Steinhauser, J. I. Polzin, F. Feldmann, M. Hermle, J. D. Murphy, S. P. Phang, W. Kwapil, M. C. Schubert, *Sol. Energy Mater. Sol. Cells* **2018**, *185*, 252-259.

[17] A. Cuevas, D. Yan, *IEEE J. Photovolt.* **2013**, *3*, 916-923.

[18] B. Hoex, J. J. H. Gielis, M. C. M. v. d. Sanden, W. M. M. Kessels, *J. Appl. Phys.* **2008**, *104*, 113703.

[19] H. Lee, T. Tachibana, N. Ikeno, H. Hashiguchi, K. Arafune, H. Yoshida, S.-i. Satoh, T. Chikyow, A. Ogura, *Appl. Phys. Lett.* **2012**, *100*, 143901.

[20] G. von Gastrow, S. Li, M. Putkonen, M. Laitinen, T. Sajavaara, H. Savin, *Appl. Surf. Sci.* **2015**, *357*, 2402-2407.

[21] A. Delabie, S. Sioncke, J. Rip, S. Van Elshocht, G. Pourtois, M. Mueller, B. Beckhoff, K. Pierloot, *J. Vac. Sci. Technol. A* **2011**, *30*, 01A127.

[22] D.-H. Kim, S.-B. Baek, Y.-C. Kim, *Appl. Surf. Sci.* **2011**, *258*, 225-229.

[23] A. M. Albadri, *Thin Solid Films* **2014**, *562*, 451-455.

[24] J. Schmidt, B. Veith, F. Werner, D. Zielke, R. Brendel, Silicon surface passivation by ultrathin Al2O3 films and Al2O3/SiNx stacks, 35th IEEE Photovoltaic Specialists Conference, Honolulu, Hawaii, **2010**, pp. 000885-000890.

[25] M. N. Getz, M. Povoli, E. Monakhov, *J. Appl. Phys.* **2021**, *129*, 205701.

[26] K. R. McIntosh, L. E. Black, *J. Appl. Phys.* **2014**, *116*, 014503.

[27] C. M. Herzinger, B. Johs, W. A. McGahan, J. A. Woollam, W. Paulson, *J. Appl. Phys.* **1998**, *83*, 3323-3336.

[28] F. Campabadal, O. Beldarrain, M. Zabala, M. C. Acero, J. M. Rafí, Comparison between Al2O3 thin films grown by ALD using H2O or O3 as oxidant source, Proceedings of the 8th Spanish Conference on Electron Devices, CDE'2011, Palma de Mallorca, Spain, **2011**, pp. 1-4.

[29] S. E. Potts, G. Dingemans, C. Lachaud, W. M. M. Kessels, *J. Vac. Sci. Technol. A* **2012**, *30*, 021505.

[30] K. DE, S. RM, *18th IEEE Photovoltaic Specialists Conference, Las Vegas* **1985**, 578.

[31] M. J. Kerr, A. Cuevas, *J. Appl. Phys.* **2002**, *91*, 2473-2480.

[32] G. Dingemans, V. d. Sanden, W. Kessels, *Electrochem. Solid-State Lett.* **2010**, *13*.

[33] H. Huang, J. Lv, Y. Bao, R. Xuan, S. Sun, S. Sneck, S. Li, C. Modanese, H. Savin, A. Wang, J. Zhao, *Data in Brief* **2017**, *11*, 19-26.

[34] G. Dingemans, N. M. Terlinden, M. A. Verheijen, M. C. M. v. d. Sanden, W. M. M. Kessels, *J. Appl. Phys.* **2011**, *110*, 093715.

[35] W. A. Hill, C. C. Coleman, *Solid·State Electron.* **1980**, *23*, 987-993.

[36] R. Hezel, K. Jaeger, *J. Electrochem. Soc.* **1989**, *136*, 518-523.

[37] J. Benick, A. Richter, T. A. Li, N. E. Grant, K. R. McIntosh, Y. Ren, K. J. Weber, M. Hermle, S. W. Glunz, Effect of a post-deposition anneal on Al2O3/Si interface properties, 2010 35th IEEE Photovoltaic Specialists Conference, Honolulu, Hawaii, **2010**, pp. 000891-000896.

[38] R. L. Puurunen, *J. Appl. Phys.* **2005**, *97*, 121301.

[39] R. L. Puurunen, W. Vandervorst, W. F. A. Besling, O. Richard, H. Bender, T. Conard, C. Zhao, A. Delabie, M. Caymax, S. D. Gendt, M. Heyns, M. M. Viitanen, M. d. Ridder, H. H. Brongersma, Y. Tamminga, T. Dao, T. d. Win, M. Verheijen, M. Kaiser, M. Tuominen, *J. Appl. Phys.* **2004**, *96*, 4878-4889.

[40] M. M. Frank, Y. J. Chabal, M. L. Green, A. Delabie, B. Brijs, G. D. Wilk, M.-Y. Ho, E. B. O. d. Rosa, I. J. R. Baumvol, F. C. Stedile, *Appl. Phys. Lett.* **2003**, *83*, 740-742.

[41] D. D. M. Wayner, R. A. Wolkow, *J. Chem. Soc., Perkin Trans. 2* **2002**, 23-34.

[42] B. Gokce, E. J. Adles, D. E. Aspnes, K. Gundogdu, *Proceedings of the National Academy of Sciences* **2010**, *107*, 17503-17508.

[43] N. E. Grant, A. I. Pointon, R. Jefferies, D. Hiller, Y. Han, R. Beanland, M. Walker, J. D. Murphy, *Nanoscale* **2020**, *12*, 17332-17341.

[44] Z. Chen, P. Dong, M. Xie, Y. Li, X. Yu, Y. Ma, *J. Mater. Sci.: Mater. Electron.* **2019**, *30*, 1148-1152.

[45] S. W. Lim, F. Machuca, H. Liao, R. P. Chiarello, R. C. Helms, *J. Electrochem. Soc.* **2000**, *147*, 1136.

[46] A. Richter, J. Benick, A. Kimmerle, M. Hermle, S. W. Glunz, *J. Appl. Phys.* **2014**, *116*, 243501.

[47] J. Benick, B. Hoex, M. C. M. van de Sanden, W. M. M. Kessels, O. Schultz, S. W. Glunz, *Appl. Phys. Lett.* **2008**, *92*, 253504.

[48] M. Groner, F. Fabreguette, J. Elam, S. M. George, *Chem. Mater.* **2004**, *16*, 639-645.

Figures

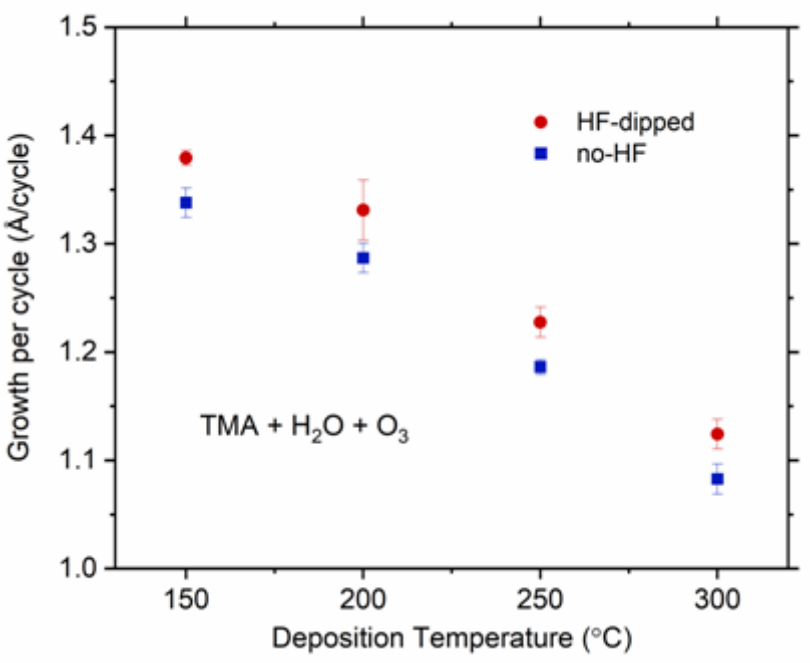

Figure 1

Growth rates of no-HF and HF-dipped samples at 150-300 ˚C for the TMA + H2O + O3 process. SE thickness measured using a model for native SiOx prior to deposition was subtracted from the final thickness before GPC was calculated.

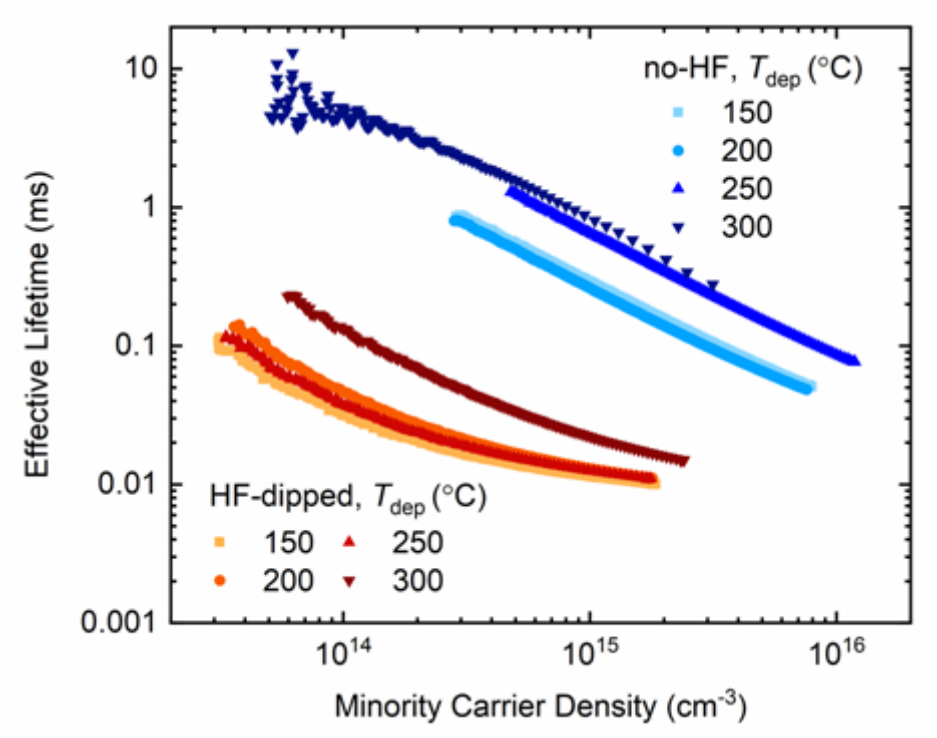

Figure 2

Effective carrier lifetime of as-deposited HF-dipped (red-scale) and no-HF (blue-scale) samples.

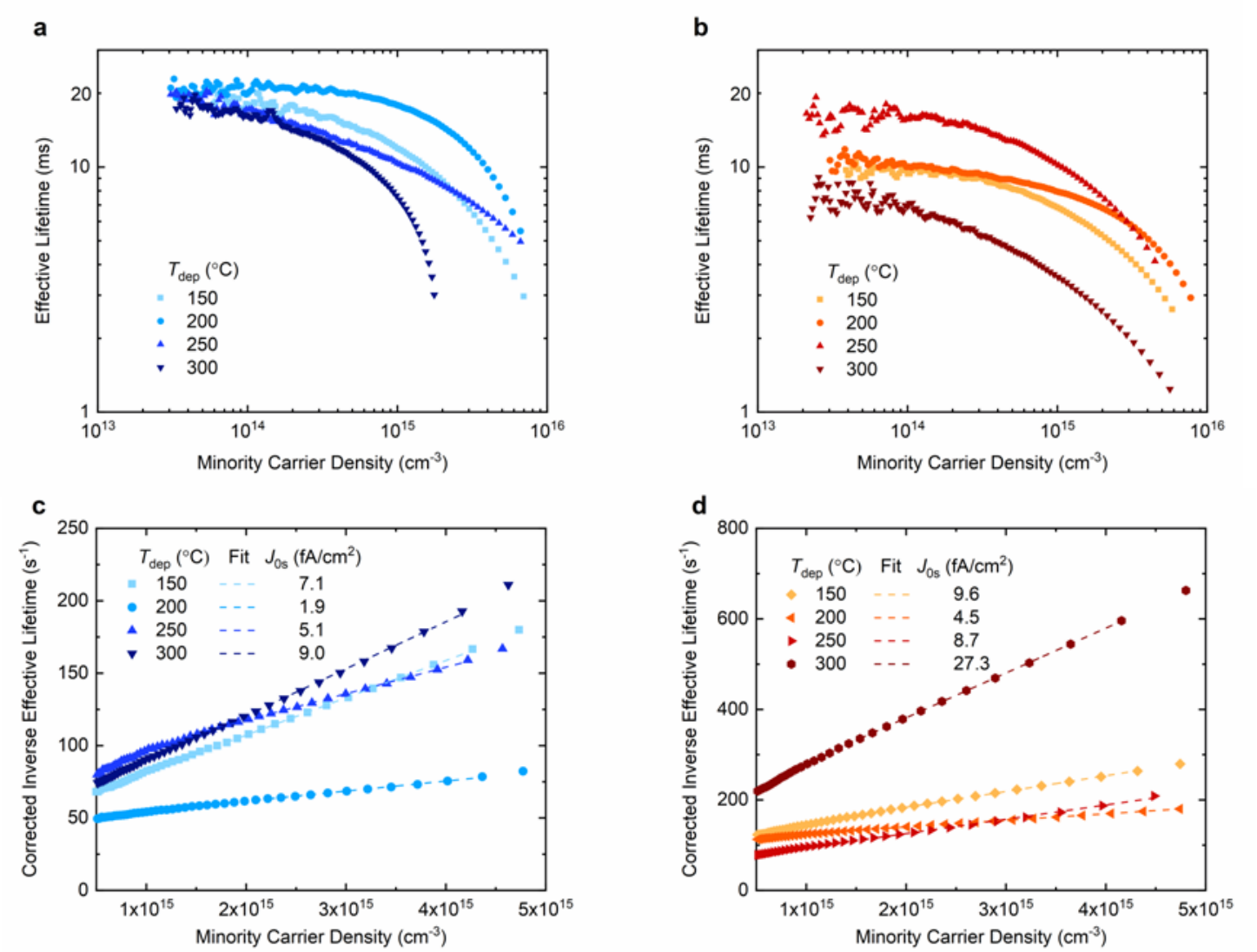

Figure 3

Effective carrier lifetime vs. minority carrier density of annealed samples deposited at different temperatures, for no-HF (a) and HF-dipped (b), and corresponding Auger-corrected inverse lifetime for no-HF (c) and HF-dipped (d), fitted with a linear fit (dashed lines) from which J0s was calculated from the slope using equation (1).

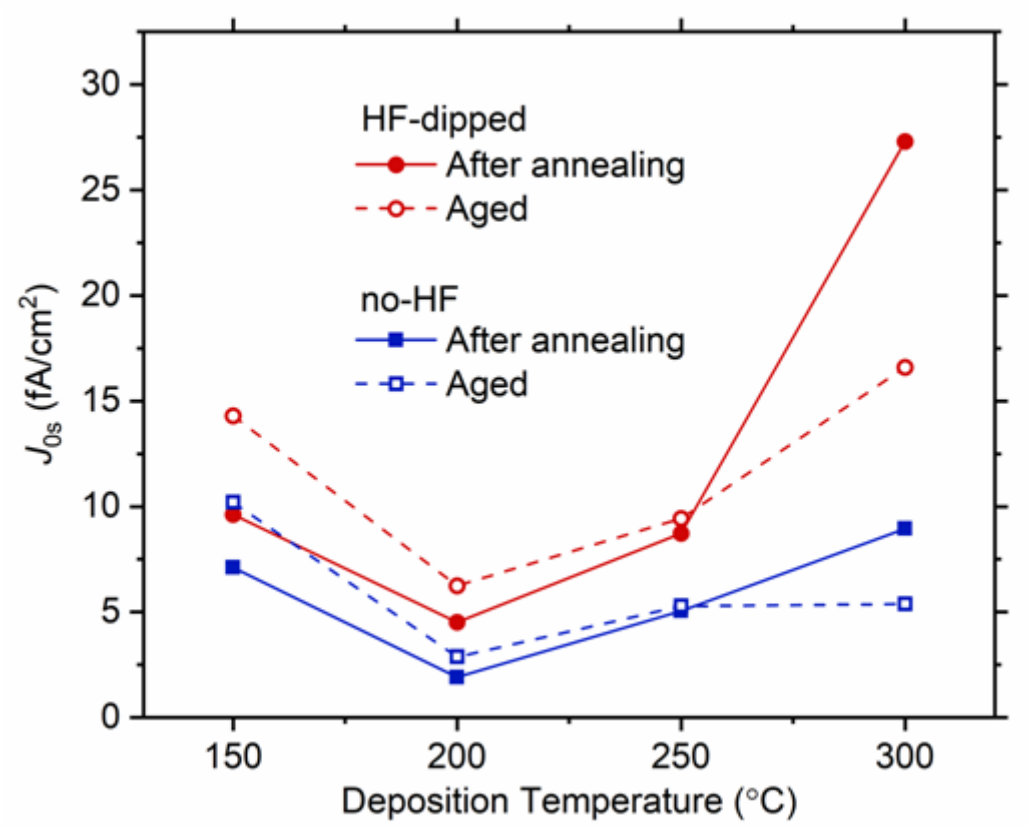

Figure 4

J0s for each deposition temperature for HF-dipped and no-HF samples, 10 min after anneal (filled), and after storing for ca. 8 months in a cleanroom (open).

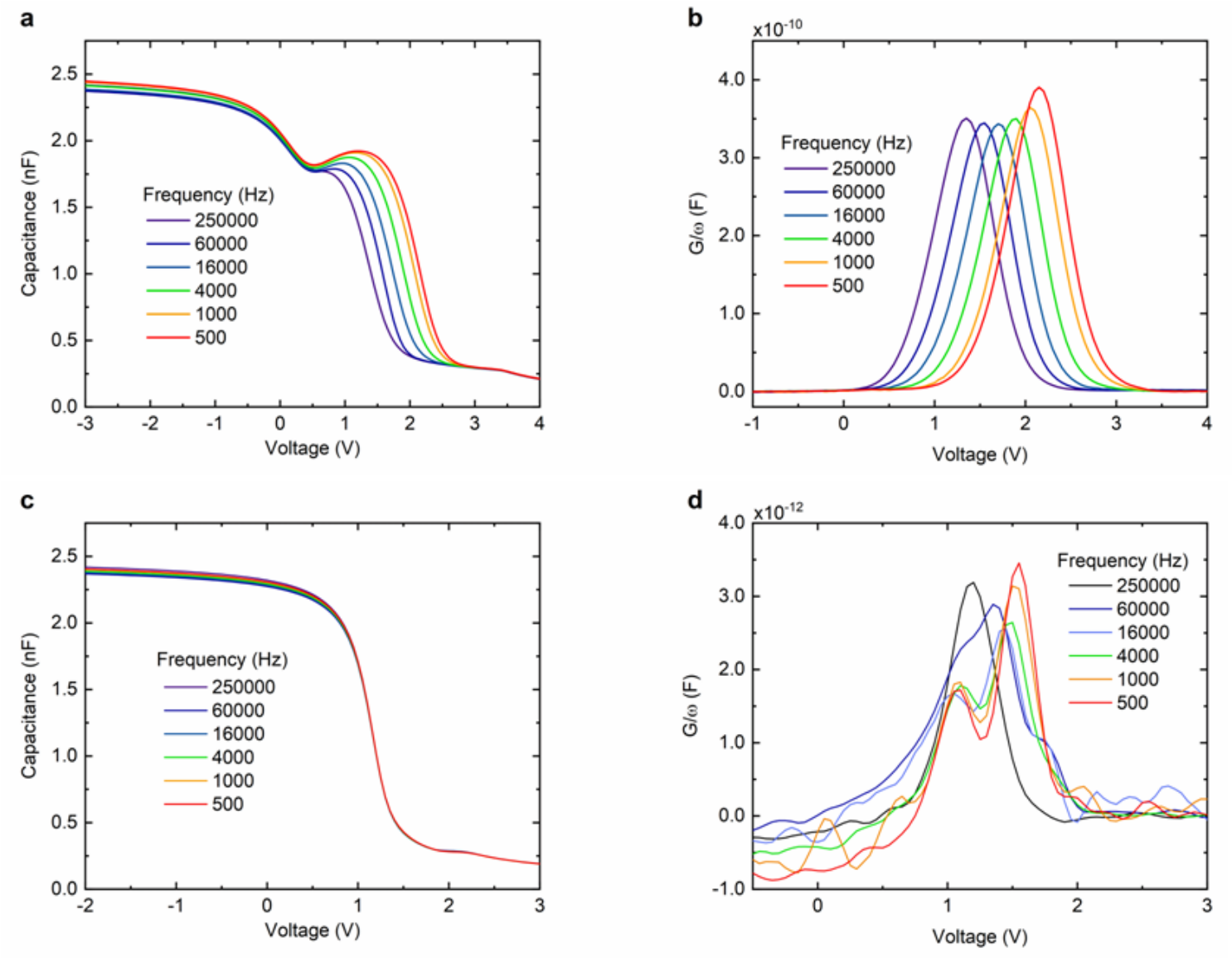

Figure 5

(a) CV characteristics as-deposited, (b) GV characteristics as-deposited, (c) CV characteristics annealed, and (d) GV characteristics annealed, of a no-HF sample deposited at 200 ˚C.

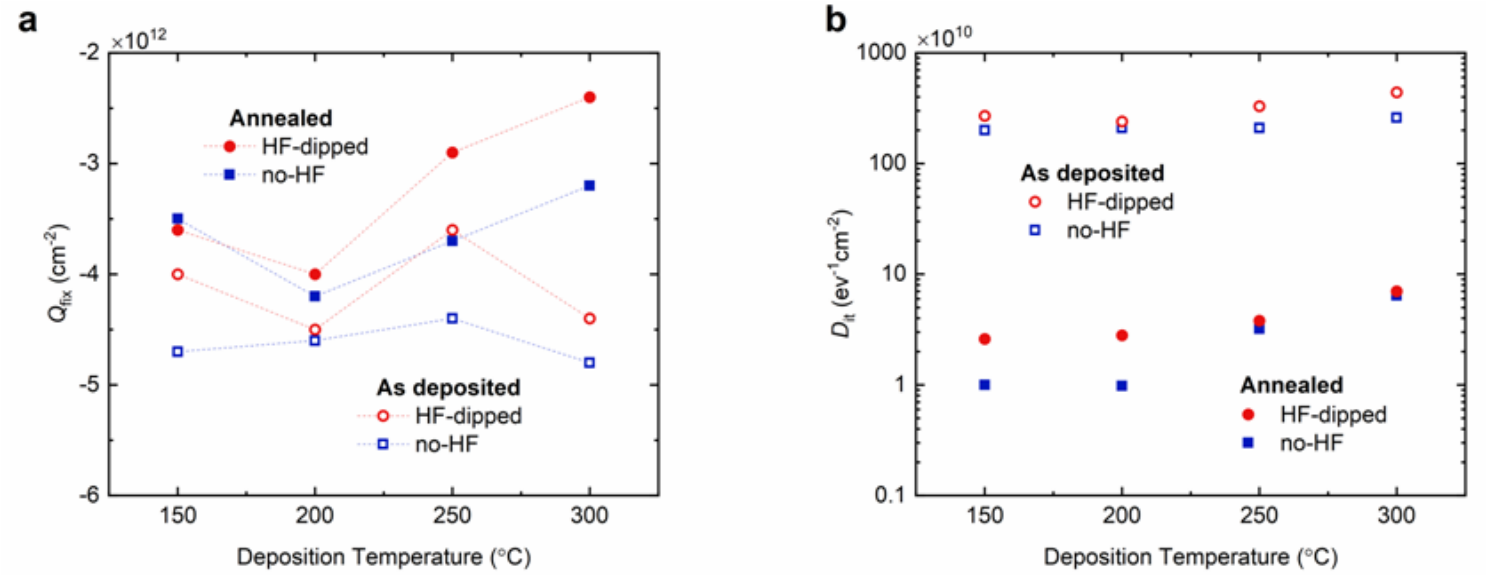

Figure 6

Qfix(a) and Dit (b) for HF-dipped (red) and no-HF (blue) for as-deposited samples (open) and annealed samples (filled), deposited at different temperatures. The 150 ˚C data points are from ref. [25].Dashed lines serve as guides for the eye.

Supplementary Files

This is a list of supplementary files associated with this preprint. Click to download.

- SupplementaryInformationImprovedsurfpassSinativeox.docx